# Quantum transport in graphene nanoribbons patterned by metal masks

Chuanxin Lian, Kristof Tahy, Tian Fang, Guowang Li, Huili Grace Xing, and Debdeep Jena[a)]
*Department of Electrical Engineering, University of Notre Dame, Notre dame, Indiana 46556, USA*

(Received 20 January 2010; accepted 12 February 2010; published online 10 March 2010)

Graphene nanoribbons (GNRs) were fabricated by metal mask lithography and plasma etching. GNRs with width ~20 nm show field-effect conductance modulation of ~12 at room temperature and $>10^6$ at 4.2 K. Conductance quantization due to quantum confinement in low field transport was observed. Landauer formula was utilized to fit the experimental data and excellent agreement was obtained. The extracted subband energy separation was found to deviate from the predicted values of perfect armchair GNRs. Transmission probability is much smaller than unity due to scattering by GNR edge/bulk disorder and impurities, indicating a mean free path ~40 nm. High field family I-Vs exhibited current saturation tendency and current density as high as 2 A/mm has been measured at low temperature. © *2010 American Institute of Physics*. [doi:10.1063/1.3352559]

Graphene, a single sheet of graphite, has generated intense interest since its isolation in 2004.[1] Two-dimensional (2D) graphene sheets have zero band gap, while ultrathin graphene nanoribbons (GNRs) can show semiconducting properties with the energy band gap scaling inversely with the ribbon width. The achievable energy band gap, superior transport properties, and the planar manufacturability establish GNRs as a possible candidate for future electronic devices.[2–4] Although sub-10-nm GNRs have been demonstrated by various chemical approaches,[5–7] the ability to form GNRs lithographically will facilitate compatibility with conventional planar integrated circuit (IC) manufacturing technology. Hydrogen silsesquioxane (HSQ) is widely utilized as the etching mask to fabricate GNRs owing to its high resolution in e-beam lithography (EBL).[8,9] HSQ can be removed by buffered hydrofluoric (BHF) acid after the GNR formation. However, the normally used $SiO_2$ substrate supporting exfoliated graphene is also etched by BHF, resulting in partially suspended or damaged GNRs. This is undesirable for uniform GNR channel modulation by the back-gate through $SiO_2$. Alternative etch mask technologies should be explored to keep the $SiO_2$ substrate unaffected. In this work, we present lithographically patterned GNR using ultrathin Al metal line masks, followed by $O_2$ plasma etching. GNRs as thin as ~20 nm have been achieved using this metal mask etching (MME) technique. The technique allows scaling down to thinner GNRs in the future.

Carrier wave functions in GNRs are confined by the edge boundaries, creating a quasi-one-dimensional (1D) transport system. Energy subbands are expected to appear due to such quantum confinement leading to conductance quantization. Subband formation in 30 nm wide GNRs has been observed at low electric fields (LEF) showing the subband energy spacing ($\Delta E$) around 50 meV.[10] A larger $\Delta E$ is expected in thinner GNRs. However, a smaller $\Delta E$ was found in the 20 nm wide GNRs reported here. A GNR band structure equation is used to explain the observation taking into account the edge roughness, ribbon width fluctuation, and crystal orientation mixture. Besides, the carrier mean free path is estimated from the transmission probability extracted by fitting the experimental data with Landauer formula.

At high electric fields (HEF), the current-carrying capacity of 1D semiconductors is determined by the longitudinal optical (LO) phonon energy in the limit of ultrafast electron-optical phonon interaction and diffusive transport.[11] Owing to the large LO phonon energy (~160 meV), GNRs are expected to be able to exhibit large saturation current while at the same time providing as-designed planar patterning which is currently not achievable with carbon nanotubes (CNTs). Field effect transistors fabricated on the GNRs reported here show current saturation tendency with the maximum current density reaching 2 A/mm at HEF (75 kV/cm).

GNRs were fabricated on exfoliated graphene flakes on $SiO_2/Si$ substrates in this work. The oxide thickness is 300 nm and the Si substrate is heavily n-type doped. Al metal masks were patterned by EBL and e-beam metal deposition. The exposed graphene was removed by $O_2$ plasma etching and the metal masks were removed by Al etchant. GNRs connected to two 2D graphene regions were thus achieved. Figure 1(a) shows the scanning electron microscopy (SEM) images of a 29 nm wide Al strip mask (top) and a 20 nm wide GNR (bottom). The fact that the obtained GNR is thinner than the Al mask indicates lateral etching in $O_2$ plasma, which suggests that the MME technique can be potentially used to achieve sub-10 nm GNRs by shrinking the Al line

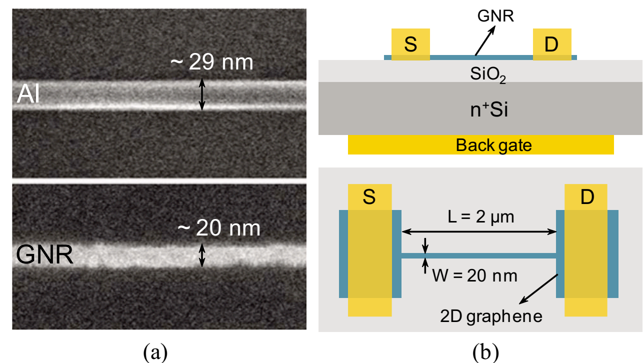


FIG. 1. (Color online) (a) SEM image of an Al strip (top) and a GNR (bottom) formed using the Al strip as etching mask; (b) Device structures and layout.

[a)]Electronic mail: djena@nd.edu.



Author complimentary copy. Redistribution subject to AIP license or copyright, see http://apl.aip.org/apl/copyright.jsp

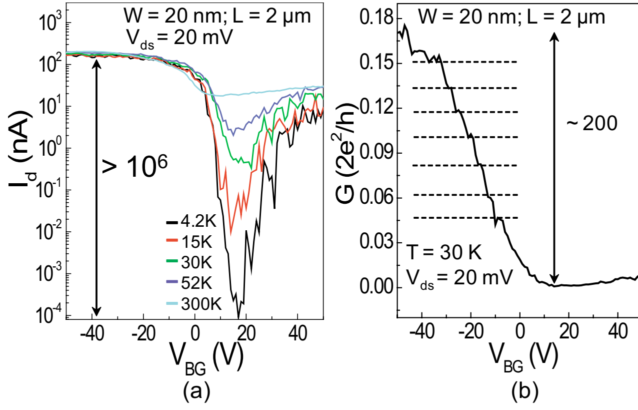


FIG. 2. (Color online) (a) Temperature-dependent transfer characteristics at 20 mV drain bias; (b) a typical transfer curve measured at 30 K showing conductance plateaus.

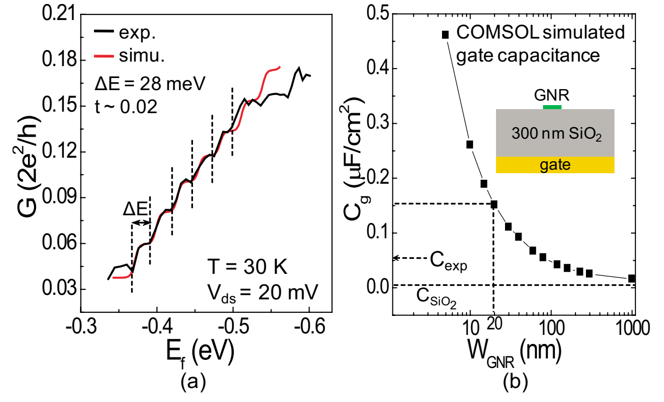


FIG. 3. (Color online) (a) Fitting of the experimental data using Landauer formula; (b) simulated gate capacitance using COMSOL.

width and modifying the plasma etching parameters. Cr/Au was e-beam deposited as source (drain) contacts on the 2D graphene areas to reduce the contact resistance. Al/Au was used as the back-gate contact. Figure 1(b) shows the device structures. The length of GNRs in this work is 2 $\mu$m. Current-voltage (I-V) measurements were performed in vacuum ($\sim 10^{-6}$ Torr) with the temperature ranging from 4.2 to 300 K.

The temperature-dependent transfer characteristics of GNRs at $V_{ds}$=20 mV are shown in Fig. 2(a). It is clearly seen that the minimum current decreases with decreasing temperature while the maximum current (due to the hole conduction) remains almost unchanged. As a result, the back-gate modulation increases from $\sim 12$ at room temperature to $>10^6$ at 4.2 K, indicating the formation of energy band gap. The positive Dirac point indicates the presence of holes at zero gate bias, possibly induced by negatively charged impurities. It is worth noting that the transfer curve does not show the symmetric V shape, with the hole conduction much stronger than the electron conduction, a phenomenon often seen in GNRs.[9,12] This is attributed to surface impurities based on the fact that surface passivation by $Al_2O_3$ grown by atomic layer deposition was found to be able to improve the electron conduction (results not shown here). But the exact origin remains unclear currently and is under investigation.

Quantum confinement in the quasi-1D GNR channel creates discrete subband energy levels, which are filled by carriers in sequence as the gate voltage increases. As a result, staircaselike features are expected in the transfer curve. The conductance quantization was indeed observed in different GNR devices and Fig. 2(b) shows a typical transfer curve measured at 30 K plotted in the linear scale exhibiting conductance plateaus with roughly equal spacing. Each 1D energy level (or mode) has a finite transmission probability. The overall device conductance $G$ at a finite temperature is the summation of all the available conducting modes, and is described by the well-known Landauer formula

$$G = \frac{2e^2}{h}\sum_i \int t_i(E)\left(-\frac{\partial f}{\partial E}\right)dE, \tag{1}$$

where $e$ is the electron charge, $h$ is the Planck constant, $t_i$ is the transmission probability of the $i$-th mode, $E$ is the electron/hole energy and $f$ is the Fermi–Dirac statistics. The nearly equal vertical spacing of the plateaus shown in Fig. 2(b) reveals that each conduction mode should have similar transmission probability. To further analyze the measured conductance quantization using Landauer formula, the back-gate voltage needs to be correlated with the Fermi energy. The link between them is the carrier density in the channel

$$C_g(V_{BG} - V_{\mathrm{Dirac}})/e = E_f^2/\pi\hbar^2 v_f^2, \tag{2}$$

where $C_g$ is effective gate capacitance per area (F/cm$^2$), $V_{BG}$ is the back gate voltage, $V_{\mathrm{Dirac}}$ is the gate voltage at the experimental minimum conductivity point, $E_f$ is the Fermi level energy, $v_f$ ($10^8$ cm/s) is the Fermi velocity, and $\hbar$ is the reduced Planck constant. This relation holds strictly in the limit of a large number of occupied subbands. Both sides of the above equation give the carrier sheet density (cm$^{-2}$) in the GNR channel.[13] The experimental data were fitted using Eq. (1), with $\Delta E$, $t$, and $C_g$ as adjustable parameters. Excellent agreement was achieved as shown in Fig. 3(a). The obtained subband energy separation from the fitting is 28 meV. To compare the extracted $\Delta E$ with theoretical prediction, we refer to GNR band structure written as follows:

$$E(k_n,k_y) = \hbar v_f\sqrt{k_n^2 + k_y^2}, \tag{3}$$

where $k_y$ is the wave vector in the GNR length direction and $k_n$ is the transverse wave vector which can only take allowed discrete values defined as $n\pi/3W$ ($n = \pm 1, \pm 2, \pm 4, \pm 5, \pm 7, \pm 8, \ldots$) for GNRs with armchair edges.[14] Therefore, perfect armchair GNRs should have quantized energy levels separated by $\pi\hbar v_f/3W$, which is 34 meV for $W$=20 nm, or two times of that value, depending on the index numbers of the two adjacent subbands. As a result, $\Delta E$ of 34 or 68 meV is expected to occur in cycle for armchair GNRs with $W$=20 nm. However, Fig. 3(a) shows nearly equal energy spacing between two close plateaus and the extracted $\Delta E$ is smaller than predicted. The discrepancy could be due to the fact that the GNRs are very likely formed with intermixing both armchair and zigzag edge orientations. The presence of zigzag edges can introduce extra allowed subband energies with $n = \pm 3, \pm 6, \ldots$, resulting in quasi-equally spaced (in energy) conductance plateaus. Besides, the fabricated GNRs have rough edges, as shown in Fig. 1(a), causing edge states and width variation which perturb the real band structure from the ideal case.

The extracted $C_g$ is 0.065 $\mu$F/cm$^2$, different from the capacitance of the 300 nm $SiO_2$ insulating layer

Author complimentary copy. Redistribution subject to AIP license or copyright, see http://apl.aip.org/apl/copyright.jsp

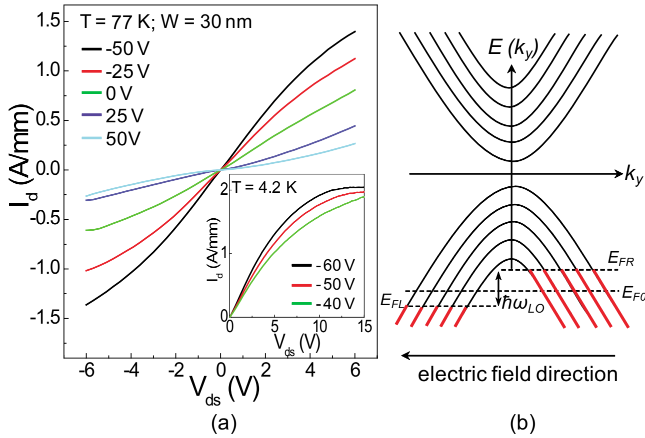


FIG. 4. (Color online) (a) High field family I-Vs measured at 77 and 4.2 K (inset); (b) sketch of subband filling at the current saturation regime.

($0.012\ \mu F/cm^2$). This is not surprising since the parallel-plate capacitor model does not apply in this case considering the ultra-small GNR width. Figure 3(b) plots the gate capacitance simulated using COMSOL software package. Quantum capacitance was neglected due to the thick oxide layer. The simulated $C_g$ for $W=20$ nm is $0.151\ \mu F/cm^2$, larger than $0.065\ \mu F/cm^2$. In the simulation, the potential was assumed to be uniform along the ribbon width direction. However, the GNR edge states could cause electrostatics perturbation, reducing the effective gate capacitance.[15]

The average transmission probability is $t \sim 0.02$, similar to that reported in Ref. 10. The very small $t$ can be explained by the scattering due to GNR edge/bulk disorder which can severely suppress the conductance causing $G$ much smaller than $2e^2/h$ (Ref. 16). Since the field in the GNR channel is relatively low (100 V/cm), the carrier mean free path λ can be estimated by $t=\lambda/(\lambda+L)$ (Ref. 17) where $L$ is the GNR channel length, giving $\lambda=40$ nm. Compared with purified CNTs which can have λ reaching a few microns, lithographically fabricated GNRs suffer from severe scattering by edge/bulk disorder and impurities either at the surface or in the substrate or both.

Figure 4(a) shows the HEF family I-Vs measured at 77 K. The source and drain electrodes were found to be exchangeable as can be seen from the symmetric I-Vs in the first and third quadrant. This is not unexpected since the back gate controls the entire GNR channel. The inset shows I-Vs measured at 4.2 K. The drain current exhibits tendency to saturate at high drain bias and the maximum current density is $\sim 2$ A/mm ($W=30$ nm) at $V_{ds}=15$ V (equivalent electric field: 75 kV/cm), indicating high current drive capability. At HEF, the energy bandwidth of current carrying electrons/holes is limited by the LO phonon energy $\hbar\omega_{LO}$ in the limit of ultrafast LO phonon scattering and diffusive transport. The saturation current carried by one subband is $2e\omega_{LO}/2\pi$ $\sim 12\ \mu A$ for GNRs.[11] Therefore, five subbands in the valence band contribute to the total saturation current (2 A/mm corresponding to $60\ \mu A$ for $W=30$ nm) as sketched in Fig. 4(b), where $E_{FR}$ and $E_{FL}$ are Fermi energies for carriers moving right and left respectively. $E_{F0}$ is the Fermi energy at equilibrium.

In summary, GNRs as thin as 20 nm have been achieved using a metal mask etching technique. The procedure can potentially be scaled to fabricate sub-10-nm GNRs lithographically. GNRs are promising for future electronic devices due to their large LO phonon energy and planar manufacturability. But the challenge is to find solutions to mitigate the edge roughness, purifying the material system, and controlling the GNR orientation, because the disorder/impurity scattering and presence of zigzag edge orientations degrade the semiconducting and transport properties. Nevertheless, even with "visible" (under SEM) roughness, the ~20–30 nm GNRs reported here show large low-temperature gate modulation and high saturation current. More encouraging results are expected in the future by improving the ribbon formation technique using metal line etching masks.

This work is financially supported by NSF Award No. ECCS-201309 and the Nanoelectronics Research Initiative (NRI) through the Midwest Institute for Nanoelectronics Discovery (MIND). The authors would like to thank Prof. Joerg Appenzeller for helpful discussions.

[1]K. S. Novoselov, A. K. Geim, S. V. Morozov, D. Jiang, Y. Zhang, S. V. Dubonos, I. V. Grigorieva, and A. A. Firsov, Science **306**, 666 (2004).
[2]Q. Zhang, T. Fang, H. Xing, A. Seabaugh, and D. Jena, IEEE Electron Device Lett. **29**, 1344 (2008).
[3]B. Huang, Q. Yan, G. Zhou, J. Wu, B. Gu, W. Duan, and F. Liu, Appl. Phys. Lett. **91**, 253122 (2007).
[4]R. Murali, K. Brenner, Y. Yang, T. Beck, and J. D. Meindl, IEEE Electron Device Lett. **30**, 611 (2009).
[5]X. Li, X. Wang, L. Zhang, S. Lee, and H. Dai, Science **319**, 1229 (2008).
[6]D. V. Kosynkin, A. L. Higginbotham, A. Sinitskii, J. R. Lomeda, A. Dimiev, B. K. Price, and J. M. Tour, Nature (London) **458**, 872 (2009).
[7]L. Jiao, L. Zhang, X. Wang, G. Diankov, and H. Dai, Nature (London) **458**, 877 (2009).
[8]M. Y. Han, B. Oezyilmaz, Y. Zhang, and P. Kim, Phys. Rev. Lett. **98**, 206805 (2007).
[9]Z. Chen, Y. Lin, M. J. Rooks, and P. Avouris, Physica E **40**, 228 (2007).
[10]Y. Lin, V. Perebeinos, Z. Chen, and P. Avouris, Phys. Rev. B **78**, 161409 (2008).
[11]D. Jena, J. Appl. Phys. **105**, 123701 (2009).
[12]X. Wang, X. Li, L. Zhang, Y. Yoon, P. K. Weber, H. Wang, J. Guo, and H. Dai, Science **324**, 768 (2009).
[13]T. Fang, A. Konar, H. Xing, and D. Jena, Appl. Phys. Lett. **91**, 092109 (2007).
[14]T. Fang, A. Konar, H. Xing, and D. Jena, Phys. Rev. B **78**, 205403 (2008).
[15]J. Guo, Y. Yoon, and Y. Ouyang, Nano Lett. **7**, 1935 (2007).
[16]E. R. Mucciolo, A. H. Castro Neto, and C. H. Lewenkopf, Phys. Rev. B **79**, 075407 (2009).
[17]M. Lundstrom, IEEE Electron Device Lett. **18**, 361 (1997).

Author complimentary copy. Redistribution subject to AIP license or copyright, see http://apl.aip.org/apl/copyright.jsp